Acta Crystallographica Section B
**Structural Science**
ISSN 0108-7681

# Structural phase transition and hydrogen ordering of $TlH_2PO_4$ at low temperature

**I. H. Oh,[a] M. Merz,[b]* S. Mattauch[c] and G. Heger[b]**

[a]HANARO Utilization Technology Development Division, HANARO Application Center, Korea Atomic Energy Research Institute, 150 Deokjin-dong, Yusung, Daejon, Korea 305-353, [b]RWTH Aachen, Institut für Kristallographie, Jägerstrasse 17-19, D-52056 Aachen, Germany, and [c]Forschungszentrum Jülich, Institut für Festkörperforschung, D-52425 Jülich, Germany

Correspondence e-mail: merz@xtal.rwth-aachen.de

Received 19 August 2005
Accepted 16 May 2006

The crystal structure of $TlH_2PO_4$ (TDP) has been studied at low temperature. The lattice parameters were derived from high-resolution X-ray powder diffraction in the temperature range between 8 and 300 K. A detailed crystal structure analysis of the antiferroelectric low-temperature phase TDP-III has been performed based on neutron diffraction data measured at 210 K on a twinned crystal consisting of two domain states. The structure model in the triclinic space group $P\bar{1}$ is characterized by a complete ordering of all the H atoms in the asymmetric O—H···O hydrogen bonds. The phase transition from the ferroelastic TDP-II to the antiferroelectric TDP-III phase at 229.5 ± 0.5 K is only slightly of first order and shows no detectable hysteresis effects. Its mechanism is driven by the hydrogen ordering between the partially ordered TDP-II state and the completely ordered TDP-III state. The polymorphism of TDP and the fully deuterated $TlD_2PO_4$ (DTDP) is presented in the form of group–subgroup relations between the different space groups.

## 1. Introduction

$TlH_2PO_4$ (thallium dihydrogen phosphate, TDP) and its deuterated form $TlD_2PO_4$ (deuterated thallium dihydrogen phosphate, DTDP) belong to the large structure family of the type $A(H,D)_2PO_4$ ($A$ = $K^+$, $Rb^+$, $Cs^+$, $Tl^+$ *etc.*) with remarkable ferroic properties related to the ordering of the H, D atoms in short O—(H,D)···O hydrogen bonds of length *ca* 2.5 Å. The most prominent representative of the hydrogen-bonded ferroelectrics is $KH_2PO_4$ (potassium dihydrogen phosphate, KDP), whose crystal structure has been extensively studied previously (Nelmes *et al.*, 1987; Nelmes, 1988; McMahon *et al.*, 1990). The characteristic feature of the KDP structure is a three-dimensional network of $PO_4$ groups linked by hydrogen bonds. In its paraelectric phase at room temperature, KDP has the space group $I\bar{4}2d$ and all the H atoms are dynamically disordered between almost regular $PO_4$ tetrahedra. Their distribution may be described according to the assumption of a double-well potential. In the ferroelectric phase at low temperature, however, the H atoms are ordered, thereby reducing the symmetry to $Fdd2$. Related to the formation of $[H_2PO_4]^-$ ions, a deformation of the $PO_4$ groups results which gives rise to a spontaneous polarization along the [001] direction. For the $A(H,D)_2PO_4$ family, on the one hand, three-dimensional networks of hydrogen bonds can exist as in the case of ferroelectric KDP, $KD_2PO_4$ (DKDP), and for $RbH_2PO_4$ (RDP) at room temperature and below; on the other hand, double layers of hydrogen-bonded $PO_4$ groups, *i.e.* two-dimensional networks, are formed for TDP, DTDP, $RbD_2PO_4$ (deuterated rubidium dihydrogen phosphate, DRDP) and for RDP (rubidium dihydrogen phos-

phate) at high temperature. The rich polymorphism of these compounds along with numerous phase transitions, whose mechanisms are dominated by hydrogen ordering in strong hydrogen bonds, is significantly influenced by the substitution of H with the heavy isotope deuterium (D). This so-called (H/D) isotope effect may yield very different transition temperatures [*e.g.* $T_c$(KDP) = 123 K and $T_c$(DKDP) = 213 K (Jona & Shirane, 1962)]. In the case of TDP/DTDP, RDP/DRDP the high-temperature phases are isomorphic, yet the low-temperature modifications have different symmetries.

TDP and DTDP crystallize at high temperature in the TDP-I and $\beta$-DTDP phase, respectively, both with the same orthorhombic space group $P\frac{2}{c}\frac{2_1}{a}\frac{2_1}{n}$ (Ríos, 1997; Ríos *et al.*, 1998). At 357 and 353 K structural phase transitions of different characters occur: TDP-I ($T > 353$ K) undergoes a translation-equivalent phase transition of index 2 (translationengleich t2) to TDP-II with the space group $P1\frac{2_1}{a}1$. The monoclinic structure of the ferroelastic room-temperature modificaton TDP-II is characterized by a partial hydrogen ordering in the hydrogen bonds. On the other hand, $\beta$-DTDP ($T > 357$ K) undergoes a phase transition to the antiferroelectric $\gamma$-DTDP phase, which is also of monoclinic symmetry. Its space group $P11\frac{2_1}{a}$ is connected to a doubling of the unit-cell volume with respect to TDP-II. The crystal structure of $\gamma$-DTDP is characterized by a complete ordering of the D atoms in asymmetric O—D$\cdots$O bonds.

The structural behavior of TDP at low temperature with a further phase transition at 230 K has not yet been well established. Yasuda *et al.* (1980) measured the dielectric constant and suggested that the low-temperature phase of TDP (TDP-III) is antiferroelectric. Nelmes (1981) proposed that TDP-III has a monoclinic C-centered structure with the **a** and **b** axes being doubled with respect to those of the room-temperature phase TDP-II. Hanazawa *et al.* (1991) concluded from specific heat measurements that the phase transition at $T_c$(I–II) = 357 K is of second order and the transition at $T_c$(II–III) = 230 K is first order in character. Based on optical spectroscopy, Pasquier *et al.* (1993) assumed a non-centrosymmetric symmetry of TDP-III, which would be in contradiction to antiferroelectricity. Moreover, they found an indication of an additional phase transition at *ca* 130 K. Utilizing X-ray powder diffraction, Becker (1995) revealed a triclinic symmetry for TDP-III and suggested the space group $P\bar{1}$ with a doubled unit-cell volume with respect to TDP-II. By means of optical microscopy with polarized light, Kim *et al.* (1998) observed no change of the domain structure at $T_c$(II–III). Therefore, they concluded that TDP-III remains monoclinic.

By applying second-harmonic generation measurements Álvarez-Otero *et al.* (2002) reassessed the existence of an inversion center for the TDP-III phase and performed X-ray diffraction studies on multiply twinned single crystals at low temperature. They confirmed the triclinic space group $P\bar{1}$ proposed by Becker (1995). The quality of their crystal structure analysis at 180 K, however, suffered from their use of a multiply twinned crystal having four domains. In such a case, the large X-ray absorption effects, mostly due to thallium, cannot be corrected properly. As a consequence, the location of the H atoms is not reliable in these X-ray diffraction experiments.

In order to study the mechanism of the phase transition from TDP-II to TDP-III and the role of H ordering, we have performed neutron-diffraction experiments on single crystals between room temperature and 210 K. In contrast to X-rays, neutrons are basically not absorbed by TDP. Owing to the symmetry reduction at $T_c$(II–III), the crystal becomes twinned at low temperature with only two domain states.

The evolution of the lattice parameters as a function of temperature has been determined by high-resolution X-ray powder diffraction experiments performed in the temperature range between 8 and 300 K. Further optical studies using the polarizing microscope showed a significant change of the optical birefringence at the phase transition.

## 2. Experimental

### 2.1. Sample preparation

Large single crystals of TDP were grown in the monoclinic TDP-II phase from aqueous solution by the evaporation method at room temperature. For the synthesis the reaction of $Tl_2CO_3 + 2\,H_3PO_4 = 2TlH_2PO_4 + H_2O + CO_2\uparrow$ was used. Optically perfect crystals of more than 5 mm in diameter were obtained. For the X-ray powder diffraction measurements, such crystals were ground under Ar atmosphere in order to minimize exposure to water. Attempts to prepare fine-crystalline TDP powders from the precipitate of a saturated TDP solution in acetone failed because the precipitate contained additional phases of unknown structure.

### 2.2. X-ray powder diffraction

For the determination of the lattice parameters of TDP in the temperature range 8–300 K, a high-resolution X-ray powder diffractometer, X'Pert PRO (PANalytical), was used. The primary optic of this diffractometer was composed of a parabolic X-ray mirror combined with a Ge(220) double monochromator yielding a quasi-parallel beam with Cu $K\alpha_1$ ($\lambda = 1.54056$ Å) radiation. Owing to the $\theta$–$\theta$ geometry of the diffractometer, the flat sample was fixed in the horizontal plane. The sample holder consisted of a Cu plate, which was mounted on top of a double-stage closed-cycle cooler. The diffracted beam was focused onto the detector by a secondary parabolic mirror. The cryostat was equipped with low-absorbing Mylar X-ray windows. The focusing secondary X-ray mirror ensured an extremely low background for the complete $2\theta$ range. The temperature of the sample was measured and controlled by two diode sensors with a stability of $\pm$ 0.1 K. One sensor was in direct contact with the sample holder, the other was situated close to the heater at the cold-head of the cooler. The powder sample prepared by grinding single crystals was predominantly composed of platelet-like crystallites, which were effectively oriented parallel to the sample surface. Owing to the large X-ray absorption of TDP (linear absorption coefficient $\mu = 64.80$ mm$^{-1}$ for Cu $K\alpha_1$),

**Table 1**
Temperature-dependent lattice parameters of TDP on cooling and heating.

| | $a$ (Å) | $b$ (Å) | $c$ (Å) | $\alpha$ (°) | $\beta$ (°) | $\gamma$ (°) |
|---|---|---|---|---|---|---|
| 288.8 K (cooling) | 14.293 (9) | 4.514 (3) | 6.512 (3) | 90 | 91.94 (3) | 90 |
| 249 K (cooling) | 14.267 (9) | 4.507 (5) | 6.504 (3) | 90 | 92.13 (3) | 90 |
| 233.1 K (cooling) | 14.253 (9) | 4.513 (5) | 6.499 (3) | 90 | 92.14 (3) | 90 |
| 209.1 K (cooling) | 28.483 (12) | 9.016 (5) | 6.502 (3) | 90.09 (5) | 92.21 (3) | 90.49 (3) |
| 159.4 K (cooling) | 28.418 (12) | 9.015 (5) | 6.494 (3) | 90.14 (5) | 92.38 (3) | 90.82 (5) |
| 149.4 K (cooling) | 28.400 (12) | 9.008 (5) | 6.490 (3) | 90.14 (5) | 92.40 (3) | 90.85 (5) |
| 99.6 K (cooling) | 28.356 (12) | 9.020 (5) | 6.483 (3) | 90.21 (5) | 92.53 (3) | 90.95 (5) |
| 49.8 K (cooling) | 28.311 (12) | 9.008 (5) | 6.472 (3) | 90.15 (5) | 92.60 (3) | 91.02 (5) |
| 20.2 K (cooling) | 28.300 (12) | 9.005 (5) | 6.470 (3) | 90.20 (5) | 92.62 (3) | 90.98 (5) |
| 7.7 K (cooling) | 28.302 (12) | 9.005 (4) | 6.470 (3) | 90.20 (5) | 92.62 (3) | 90.98 (5) |
| 20.8 K (heating) | 28.304 (12) | 9.004 (4) | 6.471 (3) | 90.21 (5) | 92.61 (3) | 90.97 (5) |
| 99.6 K (heating) | 28.358 (12) | 9.019 (4) | 6.482 (3) | 90.22 (5) | 92.51 (3) | 90.97 (5) |
| 149.4 K (heating) | 28.400 (12) | 9.006 (4) | 6.491 (3) | 90.13 (5) | 92.39 (3) | 90.79 (5) |
| 159.4 K (heating) | 28.420 (12) | 9.009 (4) | 6.495 (3) | 90.11 (5) | 92.37 (3) | 90.77 (5) |
| 209.2 K (heating) | 28.474 (12) | 9.008 (5) | 6.501 (3) | 90.10 (5) | 92.20 (3) | 90.59 (5) |
| 249 K (heating) | 14.266 (9) | 4.510 (4) | 6.505 (3) | 90 | 92.10 (3) | 90 |
| 296.5 K (heating) | 14.298 (6) | 4.515 (2) | 6.514 (3) | 90 | 91.83 (2) | 90 |

only the surface layer of the sample contributed to the powder diffraction pattern. For the setup used and a diffraction angle of $2\theta = 20°$, the transmission was reduced to only 10% for a depth of 5.5 µm. Accordingly, the resulting large texture effects could not be avoided. Complete powder patterns were measured in the $2\theta$ range between 10 and 70°, and refined employing the profile-matching routine of the *FullProf* program package (Rodriguez-Carvajal, 2001) in order to obtain the lattice parameters. To control the influence of the dominant (111) reflection of the monoclinic room-temperature phase TDP-II, this reflection was eliminated in a further profile refinement. The two refinements led to identical results. The lattice parameter refinements of the monoclinic TDP-II and the triclinic TDP-III phases are summarized in Table 1, where the error bars are estimated from the profile-matching refinements with and without the dominant (111) reflection. The refinements in the triclinic TDP-III phase at 99.6 K are shown as representative in Fig. 1. The temperature-dependent behavior of the lattice parameters together with that of the volume $V$ of the unit cell is depicted in Figs. 2(*a*–*g*). The lattice parameters $a$, $b$ and $c$, and the volume $V$ decreased upon cooling, while $\alpha$, $\beta$ and $\gamma$ increased. The variation of the lattice parameters $a$, $b$ and $\beta$ in Figs. 2(*a*), (*b*) and (*e*) is rather smooth at the phase transition. For the lattice parameter $c$ in Fig. 2(*c*) a linear dependence on the temperature with a similar slope is assumed for the data above and below the phase transition temperature $T_c$, which results in a jump-like discontinuity at $T_c$. Nevertheless, this is only a quite small effect and well within the error bars of the measured data. The temperature dependence of the $\alpha$ angle in Fig. 2(*d*) might also be interpreted in terms of a discontinuous behavior at $T_c$. Since no splitting occurs above $T_c$ for the relevant reflections in the high-resolution powder patterns, the data refinement for $T > T_c$ was restricted to the monoclinic $P1\frac{2_1}{a}1$ symmetry and $\alpha$, $\gamma = 90°$. Yet, refining the data measured at 233.1 K in the triclinic $C\bar{1}$ symmetry results in $a = 28.159$ (12), $b = 9.089$ (5), $c = 6.504$ (3) Å, $\alpha = 90.03$ (5), $\beta = 92.20$ (3) and $\gamma = 90.33$ (3)°, thereby showing that (despite increased correlations between the parameters for the triclinic refinement) the deviation for the $\alpha$ angle from 90° is very small and that the jump-like discontinuity shown in Fig. 2(*d*) is comparable in size to the error bars of the parameter. Therefore, only the triclinic $\gamma$ angle may be regarded as an order parameter. The solid curve in Fig. 2(*f*) is calculated according to

$$\eta = C\left(\frac{1-T}{T_c}\right)^{\beta}$$

with

$$\eta = \frac{\gamma(T) - 90°}{\gamma(0\,\mathrm{K}) - 90°}$$

and $T_c$(II–III) = 230 K. For the refinable parameters, $C = 1.068$ was obtained and the critical exponent was determined to be $\beta$

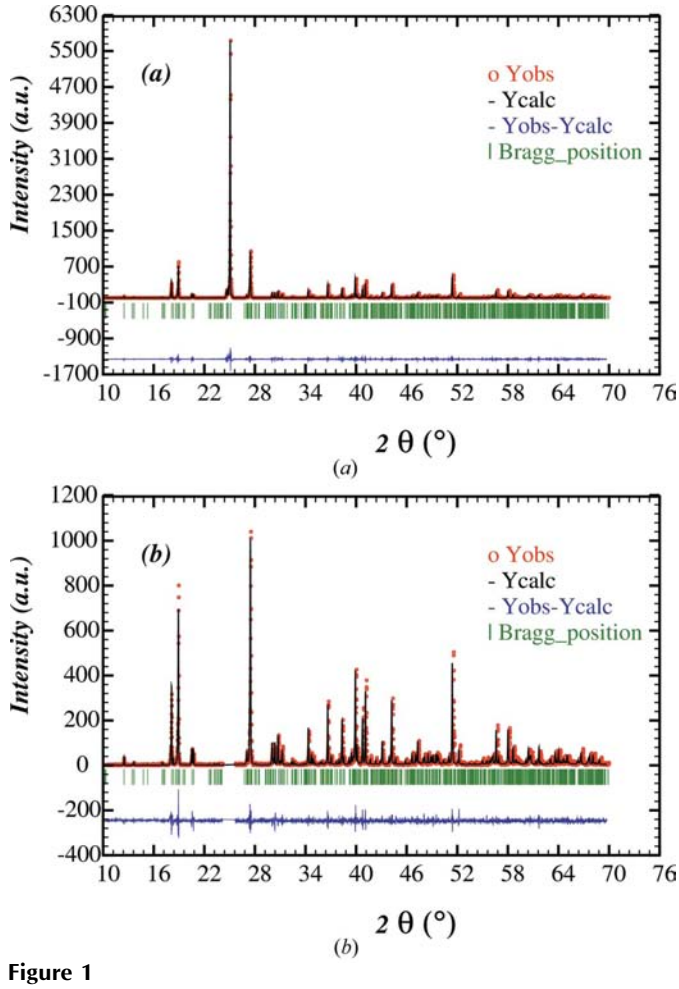


**Figure 1**
Profile matching of triclinic TDP-III at $T$ = 99.6 K (on cooling): (*a*) complete powder pattern, $R_{wp}$ = 0.061; (*b*) dominant (111) reflection excluded, $R_{wp}$ = 0.13.

= 0.255 (3). The dashed curve in Fig. 2(*f*) corresponds to a $\beta$ value of 0.5, generally assumed for phase transitions in a three-dimensional mean-field approximation. The current results apparently deviate from a mean-field behavior. Owing to the low density of the data points and the jump of the order parameter at $T_c$(II–III) it is,

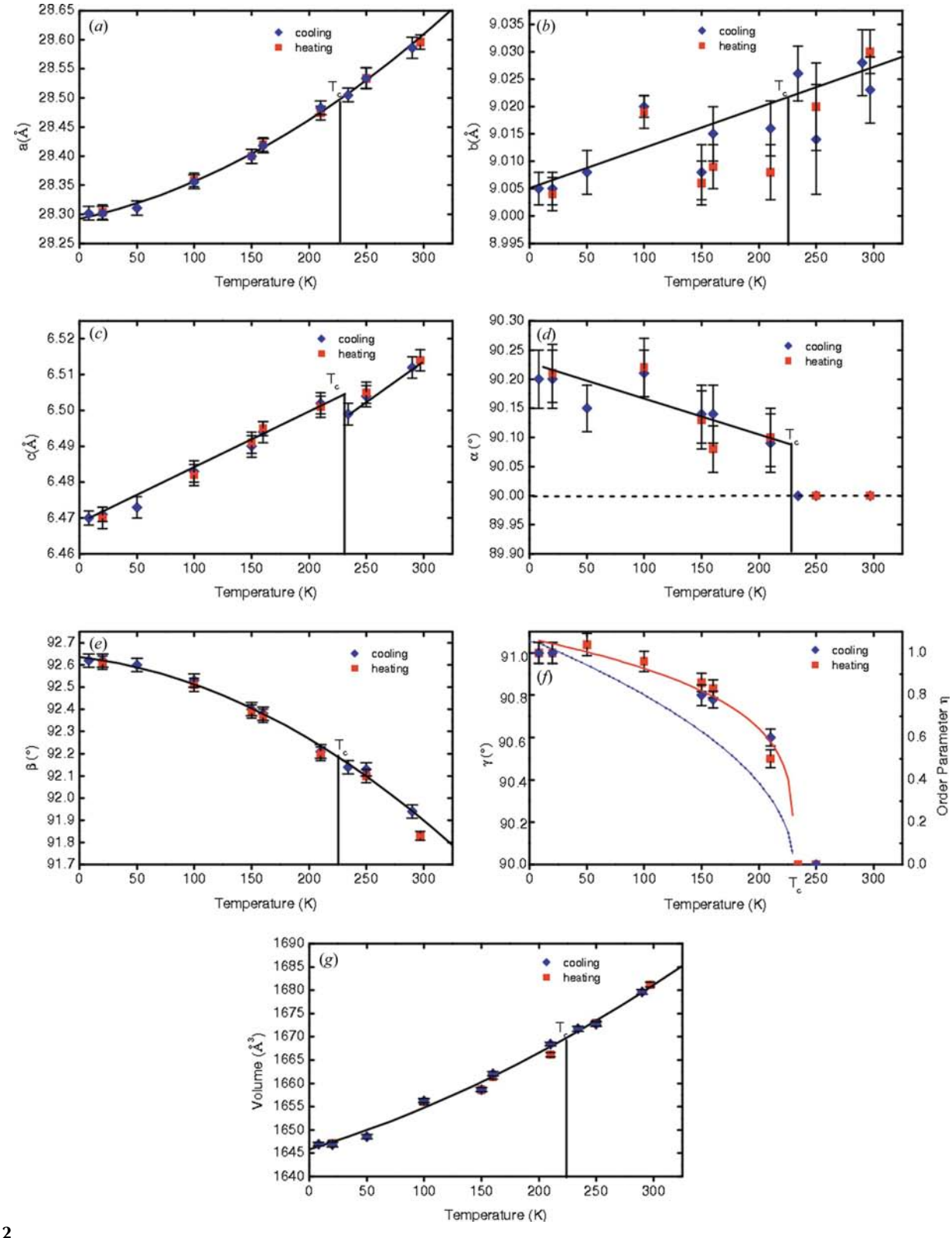


**Figure 2**
Lattice parameters and unit-cell volume of TDP as a function of temperature: (*a*) lattice parameter *a*; (*b*) lattice parameter *b*; (*c*) lattice parameter *c*; (*d*) lattice parameter $\alpha$; (*e*) lattice parameter $\beta$; (*f*) lattice parameter $\gamma$ and order parameter $\eta$; (*g*) volume of the unit cell. The solid lines in (*a*)–(*e*) and (*g*) are guides to the eye, the solid line in (*f*) is calculated with an exponent $\beta$ = 0.255 (3) and the dashed curve with $\beta$ = 0.5.

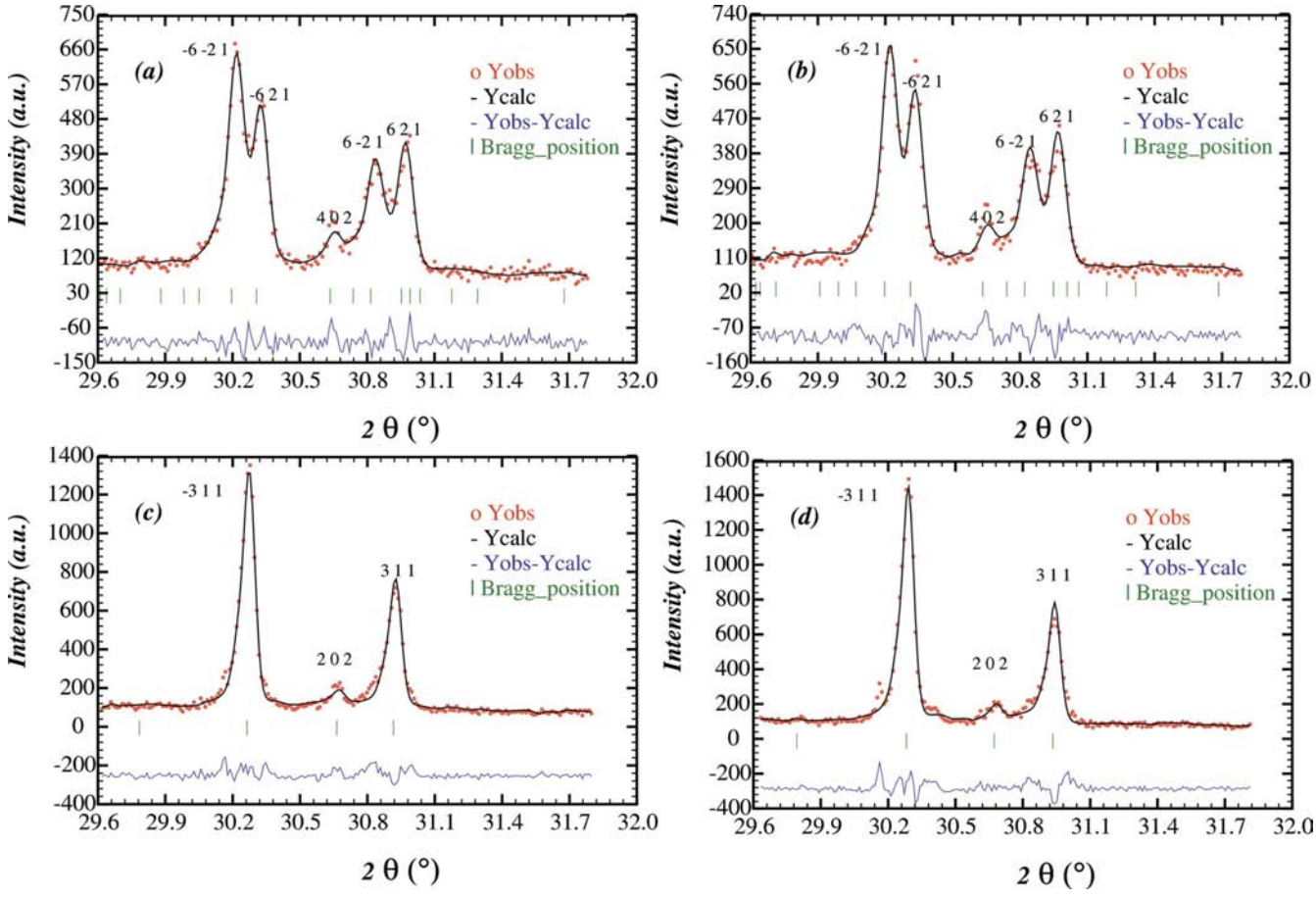


**Figure 3**
Splitting of reflections in the triclinic TDP-III phase ($C\bar{1}$): (*a*) $T$ = 223.1 K – on cooling; (*b*) $T$ = 223.1 K – on heating, compared with the monoclinic TDP-II phase ($P1\frac{2_1}{a}1$): (*c*) $T$ = 233.1 K – on cooling; (*d*) $T$ = 233.1 K - on heating.

however, not possible to discuss the critical exponent in more detail.

In the current data no evidence is found for an additional phase transition at *ca* 130 K, as previously proposed by Pasquier *et al.* (1993). More specifically, the TDP-III structure remains stable down to 8 K. In order to demonstrate the splitting of the monoclinic reflections in the triclinic TDP-III phase we have chosen the monoclinic $(\bar{3}11)_{mon}$, $(202)_{mon}$ and $(311)_{mon}$ peaks in the $2\theta$ range from 29.6 to 31.7° and investigated the temperature-dependent changes in steps of $\Delta T$ = 2 K. From the representative measurements depicted in Fig. 3 it is evident that the $(\bar{3}11)_{mon}$ reflection splits into the triclinic $(\bar{6}\bar{2}1)_{tric}$ and $(\bar{6}21)_{tric}$ reflection, $(202)_{mon}$ into $(402)_{tric}$ and $(\bar{4}02)_{tric}$, and $(311)_{mon}$ into $(6\bar{2}1)_{tric}$ and $(621)_{tric}$, completely consistent with the $P1\frac{2_1}{a}1 \rightarrow C\bar{1}$ phase transition. The powder diffraction data on cooling and heating coincide, illustrating that there are no indications of hysteresis effects at the phase transition. From the broadening/splitting of the powder reflections, produced by the splitting of the $d(hkl)$ values, we determined the temperature of the TDP II–III transition to $T_c$(II–II) = 229.5 ± 0.5 K. The superstructure reflections of the triclinic TDP-III phase are very weak and hardly visible. They cannot be used to identify the phase transition temperature. Nevertheless, from the very weak intensities of the superstructure reflections we can conclude that the thallium ions are not considerably displaced at $T_c$(II–III).

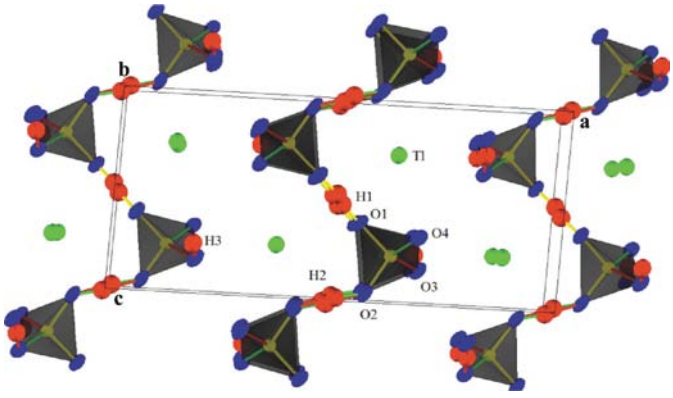


**Figure 4**
Crystal structure of TDP-II along the *b* axis at 240 K (split model).

### 2.3. Crystal structure of TDP-II

For the crystal structure investigation of TDP, a large crystal of 3 × 5 × 3 mm$^3$ was studied by neutron diffraction at the DIDO-Reactor, FZ-Jülich, Germany. Data collections were

**Table 2**
Experimental details.

| | TDP 298 K | TDP 240 K | TDP 210 K |
|---|---|---|---|
| Crystal data | | | |
| Chemical formula | $TlH_2PO_4$ | $TlH_2PO_4$ | $Tl_4H_8P_4O_{16}$ |
| $M_r$ | 301.6 | 301.6 | 1206.4 |
| Cell setting, space group | Monoclinic, $P2_1/a$ | Monoclinic, $P2_1/a$ | Triclinic, $C\bar{1}$ |
| Temperature (K) | 298 | 240 | 210 |
| $a, b, c$ (Å) | 14.331 (7), 4.535 (2), 6.514 (3) | 14.26 (2), 4.517 (9), 6.497 (10) | 28.483 (12), 9.016 (5), 6.502 (3) |
| $\alpha, \beta, \gamma$ (°) | 90, 91.67 (2), 90 | 90, 92.19 (13), 90 | 90.09 (5), 92.21 (3), 90.49 (3) |
| $V$ (Å$^3$) | 423.2 (3) | 418.2 (11) | 1668.4 (14) |
| $Z$ | 4 | 4 | 16 |
| $D_x$ (Mg m$^{-3}$) | 4.753 | 4.753 | 4.820 |
| Radiation type | Neutron | Neutron | Neutron |
| $\mu$ (mm$^{-1}$) | 0.04 | 0.04 | 0.04 |
| Crystal form, colour | Platelet, colourless | Platelet, colourless | Platelet, colourless |
| Crystal size (mm) | 5 × 3 × 3 | 5 × 3 × 3 | 5 × 3 × 3 |
| Data collection | | | |
| Diffractometer | Four-circle diffractometer | Four-circle diffractometer | Four-circle diffractometer |
| Data collection method | $\omega$ scans | $\omega$ scans | $\omega$ scans |
| Absorption correction | None | None | None |
| No. of measured, independent and observed reflections | 2766, 814, 699 | 1695, 845, 630 | 3170, 2982, 1428 |
| Criterion for observed reflections | $I > 3\sigma(I)$ | $I > 3\sigma(I)$ | $I > 2\sigma(I)$ |
| $R_{int}$ | 0.022 | 0.021 | 0.062 |
| $\theta_{max}$ (°) | 51.0 | 37.5 | 37.8 |
| No. and frequency of standard reflections | 3 every 360 min | 2 every 540 min | 2 every 540 min |
| Refinement | | | |
| Refinement on | $F^2$ | $F^2$ | $F^2$ |
| $R[F^2 > 2\sigma(F^2)]$, $wR(F^2)$, $S$ | 0.051, 0.060, 3.90 | 0.046, 0.054, 2.21 | 0.046, 0.054, 1.93 |
| No. of reflections | 699 | 699 | 2982 |
| No. of parameters | 73 | 73 | 131 |
| H-atom treatment | Refined independently | Refined independently | Refined independently |
| Weighting scheme | $w = 1/\sigma^2(F_o^2)$ | $w = 1/\sigma^2(F_o^2)$ | $w = 1/\sigma^2(F_o^2)$ |
| $(\Delta/\sigma)_{max}$ | <0.0001 | <0.0001 | <0.0001 |
| $\Delta\rho_{max}$, $\Delta\rho_{min}$ (e Å$^{-3}$) | 0.65, −0.42 | 0.51, −0.48 | 3.03, −2.28 |
| Extinction method | Secondary Type I, isotropic, Gaussian (Zachariasen, 1967) | Secondary Type I, isotropic, Gaussian (Zachariasen, 1967) | *SHELXL* |
| Extinction coefficient | 0.05425 | 0.05425 | 0.00300 (15) |

Computer programs: *PROMETHEUS* (Zucker *et al.*, 1983), *SHELXL*97 (Sheldrick, 1997), *DRAWXTAL* (Finger *et al.*, 2004).

performed on the four-circle diffractometers SV 28/1 and SV 28/2. For SV 28/1 a copper (220) monochromator wass applied to obtain a wavelength of $\lambda = 0.8724$Å, while SV 28/2 was equipped with a copper (200) monochromator to yield a wavelength of $\lambda = 1.2413$ Å. The room-temperature measurements were performed on SV 28/2, while the experiments at 240 and 210 K were conducted on SV 28/1. For the low-temperature experiments a He closed-cycle cryostat was mounted in the Eulerian cradle. The sample crystal was wrapped in Al foil in order to ensure homogeneity of the temperature. The temperature was measured and controlled by a diode sensor in direct contact with this foil. Experimental details are given in Table 2.

**2.3.1. Structure at room temperature**. In order to verify the quality of the single crystal and to examine the structural parameters obtained by Ríos (1997), we performed a structure analysis of TDP-II at room temperature. The observed reflection profiles correspond to the instrumental resolution. This demonstrates the good quality of the crystal. The systematic absences imposed by the space group $P1\,\frac{2_1}{a}\,1$ were thoroughly explored. Data were collected up to $(\sin\theta/\lambda)_{max} = 0.6207$ Å$^{-1}$ ($\lambda = 1.2413$ Å). The stability of the experiment was controlled by the repeated measurement of standard reflections. There were 2766 reflections measured and averaged over equivalents to yield a total of 814 independent reflections with an internal $R$ value of $R_{int} = 0.0212$. Reflections with $I \leq 3\sigma$ were omitted. The remaining 699 reflections were used for the structure refinements using the program packages *PROMETHEUS* (Zucker *et al.*, 1983) and *SHELXL* (Sheldrick, 1997). Starting parameters for least-squares refinements were obtained from Ríos (1997). Positional and anisotropic mean-square displacement parameters were refined, together with an overall scale factor. Extinction effects were corrected according to Zachariasen (1967; secondary type I, isotropic, Gaussian-type).

The disordered H1 and H2 atoms occupy special positions at centers of inversion ($\bar{1}$). Utilizing isotropic mean-square displacements for the refinement and with H1 and H2 at special positions, both H atoms showed large amplitudes along the corresponding O···O connection line. For this model 77

**Table 3**
Hydrogen-bond parameters (Å, °) of TDP-II.

The parameters in the first line are from the measurement at 240 K and in the second line from the measurement at room temperature.

| $A$—H—$C$ | $A$—H | H—$C$ | $A$—$C$ | Angle |
|---|---|---|---|---|
| O1—H1—O1 | 1.032 (7) | 1.422 (7) | 2.448 (7) | 172.3 (4) |
| | 1.040 (7) | 1.409 (7) | 2.445 (7) | 172.8 (4) |
| O2—H2—O2 | 1.010 (8) | 1.475 (9) | 2.483 (8) | 174.9 (6) |
| | 1.012 (6) | 1.496 (6) | 2.480 (6) | 176.2 (5) |
| O3—H3···O4 | 1.150 (6) | 1.356 (6) | 2.506 (6) | 177.2 (4) |
| | 1.176 (3) | 1.337 (3) | 2.512 (3) | 176.9 (5) |

free parameters were used. In contrast, when applying a split model for the H atoms on the special positions and isotropic displacements factors, only 73 variable parameters are needed and the refinement leads to better $R$ factors: $R_F = 0.0510$, $wR = 0.0603$ and $S = 3.90$. The refined positional and displacement parameters have been deposited.[1] They are in very good agreement ($< 3\sigma$) with the data derived by Ríos (1997). Details on the determined hydrogen bonds are listed in Table 3; the P—O bond lengths are given in Table 4. The room-temperature structure is not depicted since it is in principle identical to that shown in Fig. 4 for 240 K. In Fig. 4 the split positions of the H1 and H2 atoms are clearly visible. Concerning the hydrogen-bond lengths given in Table 3, the values for H1 and H2 refer to the split-atom model. Moreover, an interrelation exists between hydrogen ordering and the lengths of neighboring P—O bonds: the P—O3 bond with the adjacent hydrogen atom H3, which is already ordered at room temperature, is the longest while the P—O4 bond is the shortest (see Table 4). On the other hand, the P—O1 and P—O2 bond lengths with the neighboring H1 and H2 sites, respectively, have intermediate bond lengths. These findings are consistent with the bond distances and the characteristic deformation of the P—O4 tetrahedron at the phase transition, as discussed in the detailed investigations on KDP, TDP and RDP (Nelmes *et al.*, 1987; Ríos *et al.*, 1998; Mattauch *et al.*, 2004).

**2.3.2. Structure at 240 K**. For the data collection at 240 K, a total of 1695 reflections up to $(\sin\theta/\lambda)_{max} = 0.6974$ Å$^{-1}$ ($\lambda = 0.8724$ Å) were measured. After averaging over equivalents, 845 independent reflections remained ($R_{int} = 0.0207$). A total of 630 reflections which satisfied the criterion $I > 3\sigma$ were used to refine the crystal structure. Again, a slightly better residual was obtained for the split-atom model: $R_F = 0.0458$, $wR = 0.0544$ and $S = 2.21$. The positional and displacement parameters have been deposited. As a consequence of the restricted diffraction angle caused by the cryostat, not all $0k0$ reflections were accessible. This limitation is responsible for the relatively large deviations of the $U^{22}$ values from those at room temperature. The data for the hydrogen bonds are listed in Table 3, while the P—O bond lengths are given in Table 4. The structure is plotted in Fig. 4. The average temperature factors of all atoms are approximately a factor of 295 K/240 K = 1.23 smaller than those at room temperature, as might have been expected. A comparison of the 240 K results with the room-temperature refinement shows that the positional shift of all the atoms are rather small. Nevertheless, the ordering of the H3 atom increases and the splitting of the disordered hydrogen atoms H1 and H2 is more pronounced at 240 K than at room temperature. The distances between the thallium and the oxygen ions found at 240 K are slightly smaller than those observed at room temperature.

[1] Supplementary data for this paper are available from the IUCr electronic archives (Reference: LC5039). Services for accessing these data are described at the back of the journal.

**Table 4**
P—O bond lengths (Å) of TDP-II and TDP-III.

| | TDP-II | | TDP-III | |
|---|---|---|---|---|
| | 295 K | 240 K | | 210 K |
| P—O1 | 1.527 (2) | 1.529 (3) | P1—O1 | 1.57 (2) |
| | | | P4—O2 | 1.52 (2) |
| | | | P3—O3 | 1.58 (2) |
| | | | P2—O4 | 1.53 (2) |
| P—O2 | 1.532 (2) | 1.538 (3) | P1—O5 | 1.53 (2) |
| | | | P2—O6 | 1.54 (2) |
| | | | P3—O7 | 1.53 (2) |
| | | | P4—O8 | 1.58 (2) |
| P—O3 | 1.543 (2) | 1.549 (3) | P1—O9 | 1.59 (2) |
| | | | P2—O10 | 1.58 (2) |
| | | | P3—O11 | 1.53 (2) |
| | | | P4—O12 | 1.50 (2) |
| P—O4 | 1.527 (2) | 1.523 (3) | P1—O13 | 1.52 (2) |
| | | | P4—O14 | 1.53 (2) |
| | | | P3—O15 | 1.47 (2) |
| | | | P2—O16 | 1.57 (2) |
| Mean value | 1.532 (2) | 1.535 (3) | | 1.54 (2) |

### 2.4. Crystal structure of TDP-III at 210 K

The data collection at 210 K was performed up to $(\sin\theta/\lambda)_{max} = 0.7025$ Å$^{-1}$ ($\lambda = 0.8724$ Å) and a total of 3170 reflections was measured. After averaging over a small number of equivalents, according to $P\bar{1}$, 2982 symmetry-independent reflections remained ($R_{int} = 0.0621$). When applying the criterion $I > 2\sigma$, 1428 observed reflections remained for the structural refinement. For the structure refinement of the twinned crystal the twin matrix [(1 0 0), (0 −1 0), (0 0 1)] was used; the two individuals of the pseudomerohedral twin are related by a mirror plane perpendicular to **b**, which is the monoclinic axis in the higher-temperature phase. The refinements were performed with the program packages *PROMETHEUS* and *SHELXL*. The fact that each of the two twin states has a volume fraction of *ca* 50% leads to very high correlation effects and thus only an isotropic refinement is reasonable. In the enlarged unit cell [$a = 28.483$ (12), $b = 9.016$ (5), $c = 6.502$ (3) Å, $\alpha = 90.09(5)$, $\beta = 92.21$ (3), $\gamma = 90.49$ (3)°] with the space group $C\bar{1}$ (conventional space group $P\bar{1}$) all the atoms occupy general positions. There were 131 parameters refined starting from the monoclinic room-temperature structure. The final residuals were $R_F = 0.0845$, $wR = 0.1063$ and $S = 1.93$. The positional and

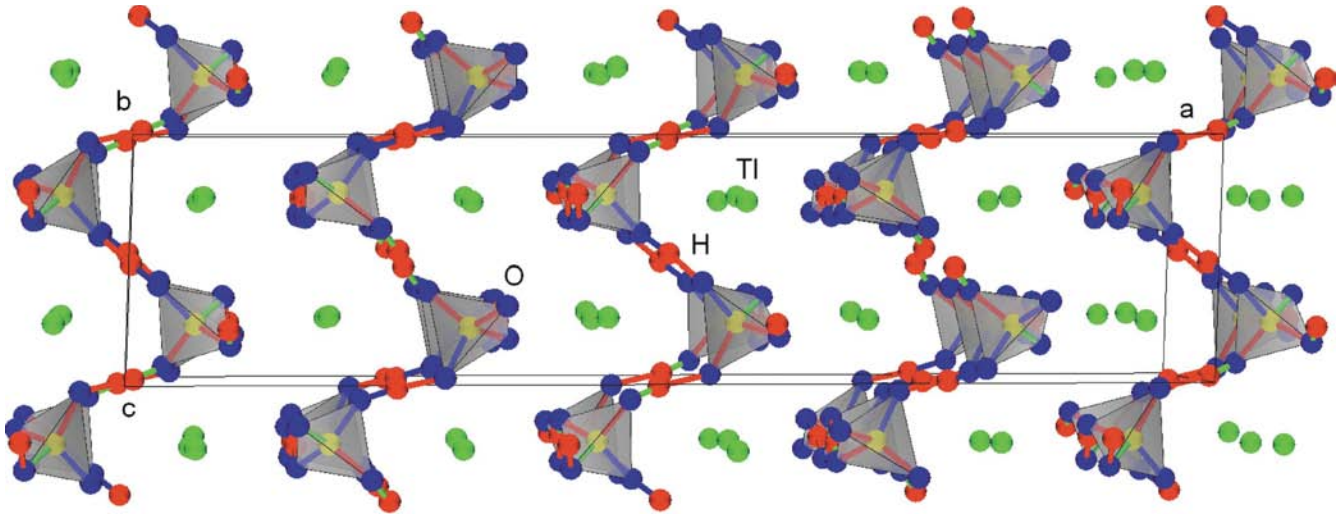


**Figure 5**
Crystal structure of TDP-III at 210 K along the **b** axis.

isotropic displacement parameters of TDP-III at 210 K have been deposited. In the TDP-III structure the H1 and H2 atoms order at one of the two disordered positions in TDP-II. Thus, all hydrogen bonds become asymmetric in TDP-III and the structure shows a complete ordering of the H atoms. This hydrogen ordering with the concomitant formation of the covalent O—H bonds causes a change of the electron density, which leads to a strong distortion of the $PO_4$ groups. In Table 4 this distortion is described by the different P—O bond distances. In Fig. 5 the crystal structure of TDP-III at 210 K is shown. Regarding the Tl—O bond distances, no substantial changes are observed at $T_c$(II–III). In both phases, TDP-II and TDP-III, the Tl—O distances show a strong variance with values between 2.8 and 3.2 Å. This finding may be explained by a prominent anisotropy of the electron density around $Tl^+$ due to lone-pair electrons. In Table 5 the lengths and the angles of the hydrogen bonds at 210 K are given.

### 2.5. TDP-II → TDP-III phase transition studied by neutron diffraction

With single-crystal neutron diffraction, the temperature-dependent measurement of selected reflections was also accomplished. Below the phase-transition temperature $T_c$(II–III), a broadening/splitting of the reflections was observed, which is related to the formation of twins owing to the symmetry reduction from monoclinic to triclinic with the consequential appearance of two twin states (Figs. 6*a* and *b*). This twinning-induced reflection splitting/broadening completely vanishes for $T > T_c$(II–III) when the monoclinic TDP-II phase reappears. Owing to the good quality of the single crystal, the intensity of strong reflections is substantially reduced in the TDP-II phase by extinction effects. The formation of twin domains at $T_c$(II–III) results in an immediate decrease of extinction at the phase transition. Even when the crystal structure is only slightly deformed at this phase transition, the reduction of the extinction effects can cause a strong enhancement for the intensity of the reflections. The rapid increase in intensity of the (802) reflection amounts to more than 100% (Fig. 6*b*) and allows a precise determination of the phase-transition temperature: $T_c = 229.5 \pm 0.5$ K. Furthermore, the reflection profile and the integral intensity

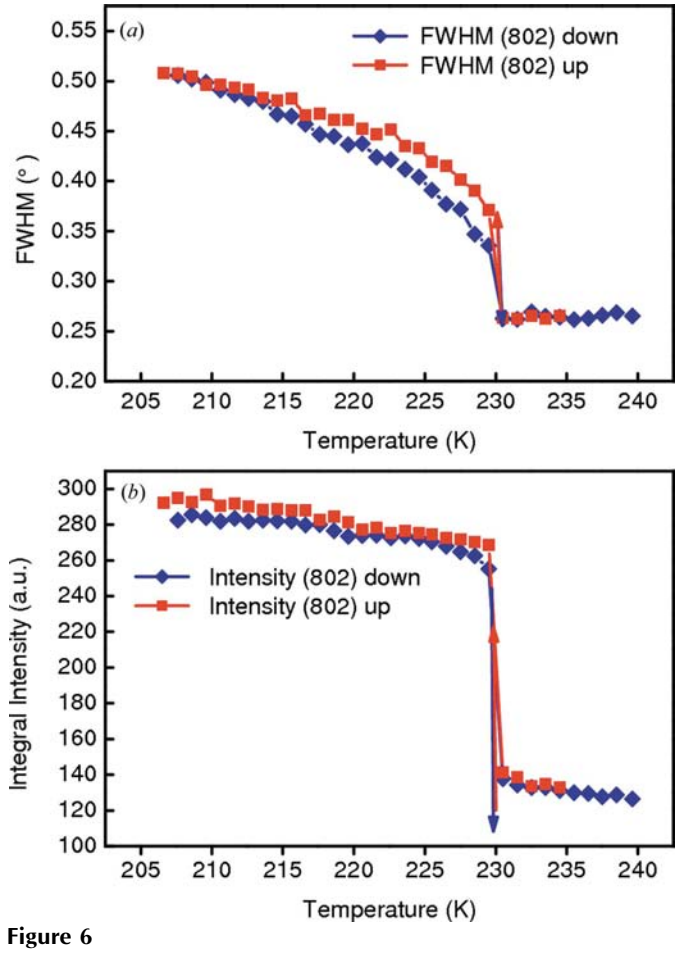


**Figure 6**
Temperature-dependent neutron diffraction study on a single crystal: (*a*) change of FWHM of the (802) reflection; (*b*) change of the integral intensity of the (802) reflection.

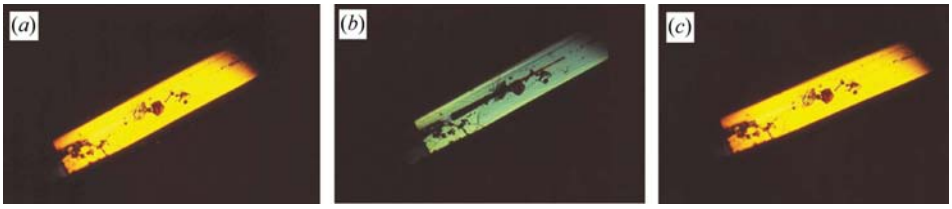


**Figure 7**
Color change at the phase transition II–III (length: 3.5 mm, width: 0.7 mm, thickness: 0.1 mm).

**Table 5**
Distances (Å) and angles (°) of hydrogen bonds of TDP-III at 210 K.

| $A$—H···$C$ | $A$—H | H—C | $A$—$C$ | Angle |
|---|---|---|---|---|
| O3—H1···O1 | 0.94 (2) | 1.51 (2) | 2.44 (3) | 167.5 (2) |
| O2—H2···O4 | 1.18 (3) | 1.28 (3) | 2.45 (1) | 167.4 (9) |
| O5—H3···O7 | 1.12 (2) | 1.30 (3) | 2.41 (1) | 169.3 (9) |
| O8—H4···O6 | 0.97 (2) | 1.64 (2) | 2.60 (9) | 173.1 (9) |
| O16—H5···O12 | 1.09 (3) | 1.42 (2) | 2.50 (2) | 170.9 (6) |
| O11—H6···O13 | 1.06 (3) | 1.52 (3) | 2.58 (2) | 172.6 (2) |
| O10—H7···O14 | 1.17 (3) | 1.32 (3) | 2.48 (2) | 168.8 (3) |
| O9—H8···O15 | 0.99 (3) | 1.42 (2) | 2.51 (2) | 173.9 (2) |

are completely reversible on heating and cooling. No evidence of hysteresis effects was found for the TDP-II → TDP-III phase transition with first-order character. Similar findings, where the reflection profile, the FWHM, the extinction effects and thus the mosaic spread completely recover when crossing the transition temperature $T_c$, were recently observed for the ferroelectric phase transition in RDP (Mattauch *et al.*, 2004). Hence, such characteristics are obviously not unique for TDP, but rather seem to be a common feature in these systems for the formation of twin domains at the (anti-)ferroelectric phase transition.

### 2.6. Optical investigation of the phase transition between TDP-II and TDP-III

The phase transition TDP-II → TDP-III was also investigated with the polarizing microscope employing crossed polarizers. The used sample crystals have a platelet-like shape with parallel surface layers perpendicular to the direction of observation. With the help of X-ray diffraction, the crystal axis perpendicular to the direction of observation was determined to be parallel to the monoclinic **b** axis. Upon cooling, the color of the crystal plate changes at *ca* 230 K from yellow to turquoise, as shown in Fig. 7. With decreasing temperature this change starts on the outer side of the crystal and continues until the entire crystal shows a uniform color. Upon heating, the reverse process is observed with the change of color beginning at the center of the crystal. This transition is completely reversible. The color change is caused by an alteration of the optical birefringence. Below $T_c$(II–III) no domain structure is observed. This points to a domain size of the twin domains which is smaller than the wavelength of light. Alternatively, it might also be possible that the used sample crystal was not twinned below $T_c$(II–III).

### 2.7. Conclusions

The crystal structure of TDP was studied in detail at low temperature. The ferroelastic TDP-II phase at room temperature is characterized by a partial hydrogen ordering in hydrogen bonds, which becomes more pronounced with decreasing temperature.

At 229.5 ± 0.5 K a phase transition of slightly first-order character occurs without any indication of hysteresis effects. The reflection splitting of the X-ray powder patterns confirms unambiguously the enlarged triclinic unit cell of the TDP-III low-temperature phase with twice the volume of TDP-II. The triclinic deformation is mostly easily observed for the $\gamma$ angle which may be regarded as an order parameter. Its temperature dependence may be described by a critical exponent $\beta$ = 0.255 (3). The TDP-III phase is stable down to 8 K. There is no evidence for a further phase transition at *ca* 130 K.

A crystal structure refinement of the TDP-III phase was performed with neutron diffraction data measured at 210 K on a twinned crystal consisting of two domain states. The triclinic structure of TDP-III in the space group $P\bar{1}$ is characterized by a complete ordering of all H atoms in asymmetric O—H···O hydrogen bonds. The covalent O—H component in the hydrogen bonds gives rise to a deformation of the electron density of the $[H_2PO_4]^-$ groups which, in effect, leads to different P—O bond lengths for the $PO_4$ tetrahedra.

The relationship between the different phases of TDP and DTDP can be described by direct group–subgroup relations

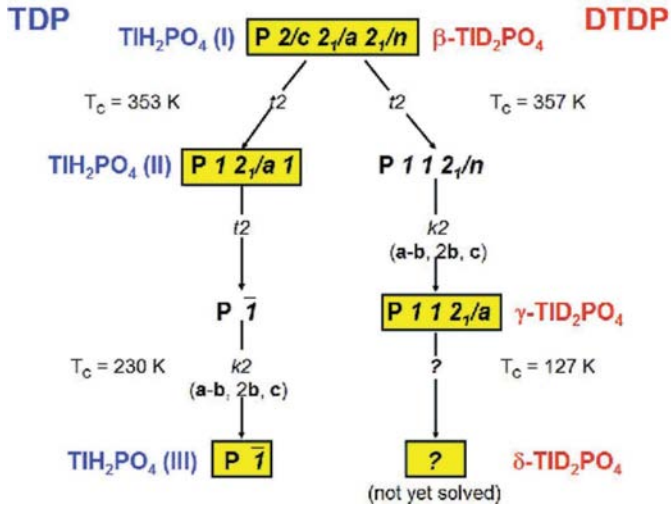


**Figure 8**
Relationship between the different phases of TDP and DTDP represented by the group–subgroup relations between the corresponding space groups.

between the corresponding space groups (Fig. 8). The polymorphism of TDP and DTDP is fundamentally different with an isomorphic high-temperature phase (TDP-I and $\beta$-DTDP), whose orthorhombic structure has the space group $P\frac{2}{c}\frac{2_1}{a}\frac{2_1}{n}$. The difference between the protonated and deuterated compounds might be regarded as an isotope effect of the $Tl(H,D)_2PO_4$ system. The group–maximum subgroup relations in Fig. 8 are marked by arrows with $t2$ and $k2$ indicating translation-equivalent (index 2) and class-equivalent (index 2) symmetry reductions, respectively. At phase transitions with translation-equivalent group–subgroup relations a twinning of the crystals may occur. For TDP the transition between the high-temperature TDP-I and the TDP-II phases ($P\frac{2}{c}\frac{2_1}{a}\frac{2_1}{n} - t2 \rightarrow P1\frac{2_1}{a}1$) leads to the appearance of ferroelastic domains with two domain states. The TDP-II $\rightarrow$ TDP-III transition is composed of two different group–max. subgroup relations: $P1\frac{2_1}{a}1 - t2 \rightarrow P\bar{1} \rightarrow k2 \rightarrow P\bar{1}$. The translation-equivalent part of index 2 ($t2$) gives rise to 180° domains in the antiferroelectric TDP-III phase, whereas the class-equivalent part of index 2 ($k2$) is associated with an enlargement of the unit-cell volume with basis vector $\mathbf{a}_{III} = \mathbf{a}_{II} - \mathbf{b}_{II}$, $\mathbf{b}_{III} = 2\mathbf{b}_{II}$ and $\mathbf{c}_{III} = \mathbf{c}_{II}$.

For DTDP the $\beta$–$\gamma$ transition is also composed of two different group–maximum subgroup relations: $P\frac{2}{c}\frac{2_1}{a}\frac{2_1}{n} - t2 \rightarrow P11\frac{2_1}{n} - k2 \rightarrow P11\frac{2_1}{a}$. In addition to the twinning due to $t2$, there is an enlargement of the unit-cell volume of $\beta$-DTDP with $\mathbf{a}_\gamma = \mathbf{a}_\beta - \mathbf{b}_\beta$, $\mathbf{b}_\gamma = 2\mathbf{b}_\beta$ and $\mathbf{c}_\gamma = \mathbf{c}_\beta$ owing to $k2$. The crystal structure of the monoclinic $\beta$-DTDP phase is characterized by a complete ordering of D atoms in asymmetric O—D···O bonds (Ríos *et al.*, 1998). Whereas the unit-cell volumes of the two antiferroelectric modifications TDP-III and $\beta$-DTDP are about the same, their space-group symmetries are principally different. Moreover, $\beta$-DTDP is not the stable phase at low temperature, since another phase transition exists at 127 K. However, the crystal structure of $\delta$-DTDP is not solved so far.

## References


Álvarez-Otero, El., Madariaga, G., Peral, I., Folcia, C. L. & Ríos, S. (2002). *Acta Cryst.* B**58**, 750–759.

Becker, M. (1995). Diplomarbeit im Fach Mineralogie, Institut für Kristallographie, RWTH, Aachen, Germany.

Finger, L., Kroeker, M. & Toby, B. (2005). *DRAWXTL*. Carnegie Institute of Washington, USA.

Hanazawa, K., Komukae, M., Okasa, T., Makita, Y., Arai, M., Yagi, T. & Sakai, A. (1991). *J. Phys. Soc. Jpn*, **60**, 188–195.

Jona, F. & Shirane, G. (1962). *Ferroelectric Crystals.* Frankfurt Am Main: Pergamon Press GmbH.

Kim, K. B., Lee, K. S. & Lee, C. E. (1998). *J. Phys. Soc. Jpn*, **67**, 1886–1889.

Mattauch, S., Heger, G. & Michel, K. H. (2004). *Cryst. Res. Technol.* **39**, 1027–1054.

McMahon, M. I., Nelmes, R. J., Kuhs, W. F., Dorwarth, R., Piltz, R. O. & Tun, Z. (1990). *Nature (London)*, **348**, 317–319.

Nelmes, R. J. (1988). *J. Phys. C Solid State Phys.* **21**, L881–L886.

Nelmes, R. J. (1981). *Solid State Commun.* **39**, 741–743.

Nelmes, R. J., Tun, Z. & Kuhs, W. F. (1987). *Ferroelectrics*, **71**, 125–141.

Pasquier, B., Le Calve, N., Al Nomsi-Teilar, S. & Fillaux, F. (1993). *Chem. Phys.* **223**, 33–50.

Ríos, S. (1997). PhD thesis, Université Paris VI, France.

Ríos, S., Paulus, W., Cousson, A., Quilichini, M. & Heger, G. (1998). *Acta Cryst.* B**54**, 790–797.

Rodriguez-Carvajal, J. (2001). *CPD Newsl.* **26**, 12–19.

Sheldrick, G. M. (1997). *SHELX*97. University of Göttingen, Germany.

Yasuda, N., Fujimoto, S. & Asano, T. (1980). *Phys. Lett.* **76**, 174–176.

Zachariasen, W. H. (1967). *Acta Cryst.* **23**, 558–564.

Zucker, U. H., Perenthaler, E., Kuhs, W. F., Bachmann, R. & Schulz, H. (1983). *J. Appl. Cryst.* **16**, 358.